International Journal of Pharmaceutics 423 (2012) 341–350

Contents lists available at SciVerse ScienceDirect

International Journal of Pharmaceutics

journal homepage: www.elsevier.com/locate/ijpharm

Crystallinity evaluation of tacrolimus solid dispersions by chemometric analysis☆

Ahmed S. Zidan[a,b], Ziyaur Rahman[a], Vilayat Sayeed[a], Andre Raw[a], Lawrence Yu[a], Mansoor A. Khan[a,*]

[a] Center for Drug Evaluation and Research, Food and Drug Administration, Silver Spring, MD, USA
[b] Department of Pharmaceutics and Industrial Pharmacy, Faculty of Pharmacy, Zagazig University, Zagazig, Egypt

ARTICLE INFO

Article history:
Received 5 September 2011
Received in revised form 1 November 2011
Accepted 3 November 2011
Available online 12 November 2011

Keywords:
Tacrolimus
Solid dispersions
Crystallinity
Near-infrared
Raman

ABSTRACT

Different destructive and nondestructive analytical methods, namely powder X-ray diffractometry (PXRD), differential scanning calorimetry (DSC), Raman and near-infrared (NIR) spectroscopy and imaging, to detect and characterize tacrolimus trace crystallinity in an amorphous solid dispersion (SD) using chemometric analysis were developed. The SD was spiked with different percentages of the crystalline drug to construct an array of SDs with different crystallinity percentages. Partial least square (PLS) regression analysis was employed to compare the performance of the calibration models created using these analytical methods. The obtained results indicated a significant interaction between tacrolimus and the employed polymer and a drug dissolution dependency on the crystalline fraction within the SDs. Using two PLS factors, these analytical methods were ranked according to its specificity to detect the trace crystallinity of SDs as NIR > PXRD > Raman > DSC. Through the application of PLS, root-mean-squared error of calibration values of 2.91%, 5.36%, 7.07% and 11.58% were calculated for the calibration models constructed by NIR, PXRD, Raman and DSC, respectively. Having a prediction error of 2.1% and a correlation coefficient of 0.99, it is demonstrated that combined NIR imaging and chemometric analysis outperformed the other methods in detecting trace crystallinity in tacrolimus amorphous systems. The spatial distributions of amorphous and crystalline drug were also obtained in order to allow for studying the crystallization dissemination in the solid dispersions. Consequently, NIR and NIR imaging coupled with chemometry was shown to be a powerful tool for the prediction of drug crystallinity within SDs.

© 2011 Elsevier B.V. All rights reserved.

1. Introduction

Tacrolimus is a widely used immunosuppressive agent isolated from *Streptomyces tsukubaensis* for treatment of organ rejection and different immunological diseases such as pulmonary fibrosis and bronchiolar asthma (Hooks, 1994; Waldrep, 1998; Loser et al., 2006). Due to its practical insolubility in water and the extensive metabolism by CYP3A4, tacrolimus is poorly tolerated and provides a variable and/or low bioavailability (Tamura et al., 2003; Venkataramanan et al., 1995, 2001). In order to enhance the oral absorption of tacrolimus, Honbo et al. (1987) reported that oily ethanol formulation and solid dispersion (SD) are the most potent among different formulations of tacrolimus examined. Amorphization is one of the mechanisms that is responsible for increasing the drug dissolution rate from SDs. The solubility advantage can only be maintained so long as conversion to the thermodynamically more stable crystalline form can be prevented (Hancock and Zografi, 1997). However, drug crystallization cannot be retarded indefinitely, and may proceed to varying degrees in SD during storage. SDs prepared with a polymer had been used to improve the physical stability of amorphous drug substances. It is well known that the nature and amounts of polymer and preparation method affect the physical properties of the drug substance in a SD (Law et al., 2001; Crowley and Zografi, 2003; Yoshihashi et al., 2006). Crystallinity of drug substance in SD is critical to the physical stability of solid dispersion (Watanabe et al., 2001). As a part of optimizing the SD formulation and the preparation process, well-focused analytical tools are needed for predicting physical stability of SDs (Yoshioka and Aso, 2007). Powder X-ray diffraction (PXRD) is widely used to evaluate the crystallinity of drug substances in SDs. However, it is not always suitable for the evaluation of lower crystallinity because of the lower detection limit (Shah et al., 2006). Differential scanning calorimetry (DSC) is also used to evaluate lower crystallinity materials by measuring thermal properties, such as glass transition temperature and/or melting point (Yonemochi et al., 1999; Miyazaki et al., 2007). But it often has difficulty in evaluating the thermal properties of drug substances in SDs due to overlapped signals originating from the other excipients as well as moisture desorption. In addition, thermal effects recorded at

☆ *Disclaimer*: The findings and conclusions in this article have not been formally disseminated by the Food and Drug Administration and should not be construed to represent any Agency determination or policy.

* Corresponding author at: Division of Product Quality Research, FDA/CDER/OPS/OTR, White Oak, LS Building 64, Room 1070, 10903 New Hampshire Ave, Silver Spring, MD 20993-002, USA. Tel.: +1 301 796 0016; fax: +1 301 796 9816.
E-mail address: Mansoor.Khan@fda.hhs.gov (M.A. Khan).

0378-5173/$ – see front matter © 2011 Elsevier B.V. All rights reserved.
doi:10.1016/j.ijpharm.2011.11.003

elevated temperatures must be interpreted cautiously and may not always be relevant under ambient conditions (Vippagunta et al., 2002).

Near-infrared (NIR), Raman and NIR imaging technology have been utilized as a process analytical technology (PAT) in various kinds of analysis of pharmaceutical products, such as the ingredient distribution and polymorph ratio within tablets and coating thickness (Elkhider et al., 2007; Lin et al., 2006). These techniques based on vibration spectroscopy make it possible to reveal physical or chemical mechanism at the molecular level. In order to evaluate the physical properties by these techniques, correct quantification of the spectra is necessary. Quantifying the spectra of multicomponent system, such as SD, is often difficult by overlapping the specific peak of drug substance and that of other excipients. NIR imaging measures a series of NIR spectra for every pixel which divides the sample into several spatial parts. A unique feature of NIR imaging technique is that it offers not only spatial distribution of components but structural information strongly related to hydrogen bonding which is one of the key factors for crystal structure (Awa et al., 2008). Imaging data having a high dimensional structure composed of two spatial and one spectral dimension is generally difficult to be directly and intuitively interpreted. As a solution for this problem, chemometric methods have often been applied to take the full advantage of the spectral and spatial information contained in the imaging data. Chemometric methods, such as partial least square regression (PLSR) and principle component regression (PCR), have been well utilized as spectra quantifying methods. PLSR method can quantify the spectra using the region which is highly correlated with differences in the physical properties of the samples (Roggo et al., 2007). On the other hand, PCR method quantifies the major spectra changes which have a possibility of not reflecting all the physical property changes. Since changes in NIR spectra often include more than one different physical property (Tishmack et al., 2003; Berendt et al., 2006), PLSR was deemed suitable for estimating the crystallinity contribution within spectra in this study.

Historically, FDA has focused on purity and assay as its basis of product quality, currently, more time is and will be spent trying to address issues dealing with physical processes. For example, what effects, if any, do small changes in the evaporation, size reduction, blending, drying, pressing, coating, or other manufacturing steps have on the final quality of the SDs such as drug crystallinity. The aim of the present study was to investigate the detailed formation mechanism of the crystalline tacrolimus in SD formulations with HPMC as carrier using a high precision data obtained from NIR, Raman and NIR imaging with chemometric analysis.

2. Materials and methods

Tacrolimus monohydrate (CAS#: 104987-11-3) was supplied from AvaChem Scientific Inc. (San Antonio, Texas, USA). HPMC 2910 (6 mPas labeled viscosity) was obtained from Shin-Etsu Chemical Co., Ltd. Tokyo, Japan. HPLC grade phosphoric acid and tetrahydrofuran were purchased from VWR Scientific (Bridgeport, NJ, USA). Hydroxypropyl cellulose (HPC) (M_{wt} 80 K) was purchased from Sigma–Aldrich (St. Louis, MO, USA). Sodium lauryl sulphate (SLS), and HPLC grade acetonitrile were purchased from Fisher Scientific (Pittsburgh, PA, USA). All other materials were of analytical grade and were used as received.

2.1. Preparation of solid dispersions

SD formulation having 1:1 weight ratio of tacrolimus to HPMC was prepared by the solvent evaporation method as described by Chiou and Riegelman (1971) with brief modification. Briefly, 10 g of tacrolimus and 10 g of HPMC were accurately weighed and tacrolimus was completely dissolved in 50 ml of ethanol. Then, HPMC was swollen by ethanol, in which tacrolimus is dissolved by stirring for 1 h. Ethanol was evaporated under reduced pressure using a vacuum dryer at 40 °C. After drying, SD was pulverized using an agate mortar and pestle. The pulverized powder was classified using the sieves (size: 60 and 120 mesh), and the particle size fraction passed through sieve 60 was used for the study.

A physical mixture with the same weight ratio was prepared by pulverization with an agate mortar and pestle. The mixture passed through the sieve (size: 60 mesh) were used for the study. The SD was spiked with different proportions of the physical mixture to prepare 6 formulations, namely SD1–SD6, having different crystallinity of 100, 75, 50, 25, 5, and 0%, respectively. Within these formulations, the SD represented the amorphous drug component while the physical mixture was the crystalline fraction within the sample.

2.2. Fourier transform infrared spectroscopy

Chemical interaction that might exist between tacrolimus and HPMC in their SD formulations was done using Fourier transform infrared (FTIR) spectroscopy equipped with an attenuated total reflectance accessory (Thermo Nicolet Nexus 670 FTIR, GMI Inc., Ramsey, Minnesota, USA). Spectra were collected in transmittance mode with 50 scans and 4.0 points of resolution. OMNIC ESP software (version 5.1) was used to capture and analyze the spectra.

2.3. Powder X-ray diffraction

The crystallinities of the raw materials, physical mixture and different SDs were determined by PXRD and performed using a benchtop X-ray diffractometer (MD-10 mini diffractometer, MTI Corporation, Richmond, CA, USA) with Cu K2α rays (λ = 1.54056 Å), a voltage of 25 kV and a current of 30 mA, in flat plate $\theta/2\theta$ geometry, over the 2θ ranges 15–75. Diffraction patterns were recorded for 20 min.

2.4. Differential scanning calorimetry

Thermal properties of raw materials, physical mixture and different SDs were also investigated by DSC. Different thermograms were collected with a DSC Q2000 (TA Instruments Co., New Castle, DE, USA). The sample equivalent to 5 mg was hermetically sealed in aluminum pan. The temperature ramping rate was 10 °C/min up to 250 °C. This temperature range covered the melting point of both components. The nitrogen gas was flowing at a pressure of 20 psi to provide inert atmosphere during the measurement and prevent oxidation reactions.

2.5. Scanning electron microscopy

The powder morphology of tacrolimus, HPMC and SD6 were visualized by scanning electron microscopy (SEM, JSM-6390 LV, JEOL, Tokyo, Japan) at a working distance of 20 mm and an accelerated voltage of 5 kV. Samples were gold coated with a sputter coater (Desk V, Denton Vacuum, NJ, USA) before SEM observation under high vacuum of 45 mTorr and high voltage of 30 mV.

2.6. Dissolution study

Tacrolimus dissolution from SDs and physical mixture was studied. The effects of the dissolution parameters such as increasing the dissolution agitation to 75 rpm and presence of surfactant (0.1% SLS) in the dissolution medium on tacrolimus dissolution

from SDs were also investigated. The 6 SD formulations equivalent to 5 mg of tacrolimus filled into gelatin capsule (size 3) were inserted into a sinker and placed in the dissolution tester. A dissolution test was performed at 37 ± 0.5 °C using the paddle method at 50 rpm with 900 ml 0.005% hydroxypropyl cellulose solution adjusted to pH 4.5 with phosphoric acid. At predetermined intervals, 1.5 ml aliquot was sampled, filtered through a PTFE membrane filter (0.45 μm), diluted with mobile phase and 100 μl was injected into the HPLC system for the quantitation of solubilized drug. Experiments were performed in triplicate. The HPLC method was developed and validated as per ICH guidelines (ICH 2005). An HP 1100 (Agilent technologies, CA, USA) HPLC was fitted with quaternary pumps, autosampler, and UV detector set at a wavelength of 205 nm, and column temperature was maintained at 60 °C. The HPLC stationary phase was a reversed phase Luna C18 (2), 4.6 mm × 100 mm (2.5 μm packing) column and a C18, 4.6 mm × 2.5 mm (5 μm packing) Luna C18 guard column (Phenomenex Torrance, CA, USA). The composition of the mobile phase was ACN: water:tetrahydrofuran:phosphoric acid (58.95:40:1:0.05) and pumped isocratically at a flow rate of 1 ml/min.

2.7. Raman spectroscopy

Raman spectra were collected employing a Raman spectrometer (Sentinal Bruker optics, Woodlands, TX, USA) equipped with a thermoelectrically cooled CCD detector and a fiber optic probe (RamanProbe, InPhotonics, Norwood, MA, USA). The measurements were carried out at room temperature using a 500 mW laser source with a wavelength of 785 nm (Starbright 785S, Torsana Laser Technologies, Skodsborg, Denmark). The samples were packed in aluminum sample holders and measured with an integration time of 5 s over the Raman shift range of 220–2250 cm^{-1}. Each spectrum was the average of 40 scans. Cyclohexane was used as a reference standard to monitor wave number accuracy.

2.8. Near-infrared (NIR) analysis

For the six formulations, NIR spectra were collected using a Foss NIR systems spectrometer equipped with Rapid Content™ Analyser (AP-2020, Model 5000, Foss NIR Systems Co., MN, USA) and a diffuse reflectance apparatus over the range 1100–2500 nm. Sample analysis occurred by scanning directly through the base of the sample vials, borosilicate glass vials. Cho et al. (2005) reported that borosilicate glass is transparent to NIR beam and do not affect the obtained spectra. Spectra were collected in sextet to include any intra-sample variation, with rotation of the vials among scans to ensure representative spectra. Using ceramic standard, internal software evaluated the spectrum of the apparent reflectance. Spectral acquisition configuration for the reflectance mode involved using a tungsten–halogen lamp, quartz beam splitter and a room temperature-indium gallium arsenide (InGaAs) detector.

2.9. Data analysis and interpretation

Spectra were exported ASCII format for chemometric analysis in the Unscrambler software (version 9.5, CAMO ASA, Norway). Principal component analysis (PCA) was performed before PLSR models were developed. PCA was used to examine any relevant and interpretable structure in the data as well as outlier detection (Naes et al., 2002). For NIR or Raman spectra, calibration models were developed using PLS regressions with full cross-validation. The optimum number of PLS factors was determined as indicated by the lowest number of factors that gave the closest to minimum value of the prediction residual error sum of squares (PRESS) function in full cross-validation, in order to avoid over-fitting of the models (Naes et al., 2002; Adams, 1995). The second derivative of the spectral data was used as a mathematical treatment to correct for baseline effects and to separate overlapping peaks and it was performed using Savitzky–Golay transformation and smoothing (11 smoothing points and third polynomial order filtering). Statistics calculated for the calibrations included coefficients of determination in cross-validation (R^2_{val}) and the root mean standard error of cross-validation (RMSEV). The prediction accuracy of the models was tested on the validation set using the standard error of prediction (SEP), bias, slope and the coefficient of correlation (Naes et al., 2002; Adams, 1995).

2.10. NIR-imaging analysis

NIR images were acquired using a Sapphire imaging system (Spectral Dimensions Inc., Olney MD) equipped with an InSb focal plane array detector (FPA) operating in the spectral region 1200–2450 nm at 10 nm steps with 8 coadds. For spectral acquisition, the samples were packed in aluminum sample holders and positioned in the field of view and four scans were averaged producing a complete dataset. Spectralon™ (Labsphere, Inc., North Sutton, NH), a high-reflectance standard, was used as background. Data processing was performed with ISys 5.0 (Spectral Dimensions Inc., Olney, MD). Reflectance spectra were initially processed by calculating $\log 1/R$ where R is the ratio of reflectance spectra from the sample and background following subtraction of the dark camera response. Second derivative spectra were calculated using a Savitzky–Golay algorithm (13 points smoothing at third order polynomial filtering) and then mean centered and scaled to unit variance. After discarding pixels with very high reflectance corresponding to the polished aluminum holders, classification using single bands and partial least squares (PLS2) was investigated to differentiate tacrolimus content according to its amorphous or crystalline state. Truncated sub-images of 50 × 100 pixels were taken for data analysis.

3. Results and discussion

One of the intrinsic problems encountered with SD systems is the re-crystallization of the amorphous drug due to the changes in the physicochemical properties of the formulation matrix. The presence of a crystalline drug in an amorphous system not only causes a significant reduction in the dissolution rate (Breitenbach, 2002) but can also become a factor in subsequent instability of the drug (Willart and Descamps, 2008). Various parameters to achieve better stability of solid dispersions have been studied in order to delay the onset of re-crystallization of the drug including the selection of hydrophilic polymers and the use of surfactants. In the current study, HPMC was selected as a matrix as well as to stabilize the amorphous form of tacrolimus in their SD formulations. It had been reported that HPMC remarkably enhances the water-solubility of drugs compared with other water-soluble carriers and/or prevents drugs from re-crystallization (Sugimoto et al., 1982). In addition, different analytical spectroscopic approaches were investigated for its ability to detect the crystallinity of these SDs.

3.1. Fourier transform infrared spectroscopy

FTIR analysis was carried out to investigate the interaction between tacrolimus and HPMC. Fig. 1 shows the FTIR spectra of the individual components, their 1:1 (w/w) physical mixture, and SD prepared by the solvent evaporation technique. The raw tacrolimus FTIR spectrum showed absorption bands of esteric CO stretch at 1194 cm^{-1}, C=C stretch at 1637 cm^{-1}, resonating amidic C=O and ketonic C=O stretching vibrations at 1738, 1728 and 1698 cm^{-1},

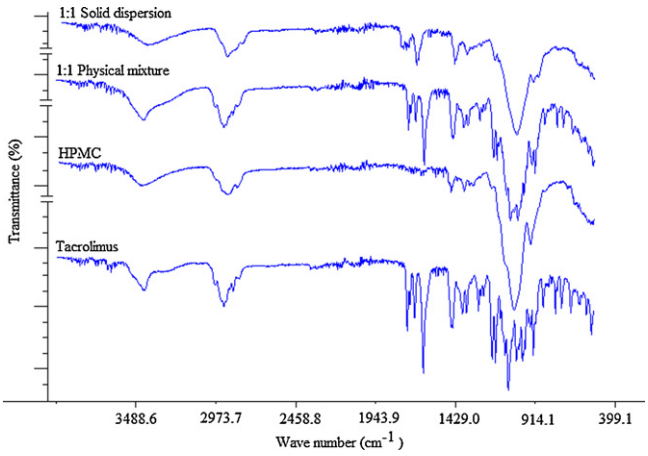

Fig. 1. FTIR spectra of raw tacrolimus, raw HPMC, 1:1 (w/w) physical mixture and 1:1 SD of tacrolimus and HPMC.

OH broad medium intensity stretch at 3450 cm^{-1}, and the etheric CO pair of stretches at 1176 and 1094 cm^{-1} (Hane et al., 1992). HPMC showed spectrum with a characteristic peak at 3430 cm^{-1} due to OH stretch. The physical mixture spectrum showed the same peaks of both components to indicate no interaction existed among them. On the other hand, the bands due to the esteric CO stretching vibration of tacrolimus in SD were different from those of physical mixtures. The absorption bands at 1698 and 1638 cm^{-1} were shifted up to 1715 and 1651 cm^{-1}, respectively, while the stretching band attributed to CO groups at 1728 cm^{-1} disappeared. These results suggested that the method employed for SD preparation resulted in a significant interaction between the CO and OH functional groups of tacrolimus with HPMC at the working compositional ratio in SD (Kushida et al., 2002).

3.2. Shape and surface morphology

Scanning electron micrographs of tacrolimus and HPMC raw powders and their 1:1 solid dispersion (SD6) are shown in Fig. 2. Tacrolimus powder appeared as smooth-surfaced rectangular crystals in shape (Yamashita et al., 2003). HPMC powder was irregular fibrous shaped particles with rough surfaces. The SD of both components appeared as fibrous shaped homogeneously mixed masses that are similar to those of HPMC. These results indicated that tacrolimus in SD was absorbed by the HPMC swollen matrix with some association to the surface and was homogeneously dispersed within the HPMC at a molecular level.

3.3. Dissolution study

To increase the oral absorption of poorly water-soluble drug, it is very important to improve the rate at which drug dissolves in the gastrointestinal tract. Therefore, the dissolution of tacrolimus from its SDs (SD2–SD6) and physical mixtures (SD1) was tested and compared to that of the raw drug (Fig. 3A). For this purpose, a dissolution medium of 0.005% HPC solution (pH 4.5) at an agitation of 50 rpm was employed (nominal dissolution condition). Compared to the drug dissolution from its physical mixture (SD1), all the SDs gave higher dissolution rates. Increasing the crystalline fraction within the SDs was associated with a lower rate of dissolution and hence the SDs could be ranked as SD6 > SD5 > SD4 > SD3 > SD2. In SD formulations, the higher energy of the amorphous species as well as the close contact between the hydrophilic carrier and drug resulting from the co-precipitation could explain this result (Leuner and Dressman, 2000). Compared to the nominal conditions, increasing the agitation speed to 75 rpm caused an insignificant increase of the drug dissolution (Fig. 3B). On the other hand, the addition of surfactant (0.01% SLS) to the dissolution medium significantly enhanced the drug dissolution for all SDs (Fig. 3C). Higher agitation speed would prevent cone formation during dissolution but still did not overcome the hydrophobicity as the crystalline fraction increased within the SD. Visually, more particles floated at the surface of the dissolution medium as the crystalline fraction increased. This was improved by the addition of SLS to the dissolution medium that lowered the surface tension and improved the wettability (Chiou and Riegelman, 1971). Fig. 3D shows statistically semi-linear relationships for the percentages dissolved of tacrolimus and the theoretical crystallinity for the different dissolution parameters. Correlation coefficients of 0.9942, 0.9720 and 0.9948 were obtained for the drug dissolution at the nominal condition, 75 rpm and 0.01% SLS, respectively, indicating that the mechanism of tacrolimus dissolution from these SDs were almost the same irrespective of changing the dissolution conditions.

3.4. PXRD and DSC studies

Fig. 4A shows the PXRD patterns of tacrolimus, HPMC, their 1:1 physical mixture (SD1), and 1:1 SD formulation (SD6). Raw tacrolimus powder showed a crystalline type diffractogram with a characteristic peaks 19.3° and 23.7°. The XRD pattern of the physical mixture of tacrolimus with HPMC was similar to the XRD pattern of tacrolimus crystalline powder with lower peaks' intensities due to the dilution factor. It was confirmed that the crystallinity of tacrolimus does not change in the physical mixtures with this polymer. On the other hand, no diffraction peak from tacrolimus was observed in the diffractogram of the SD formulation (SD6) to suggest that tacrolimus exists in an amorphous state in SD6. Fig. 4B shows the DSC thermograms of tacrolimus, HPMC, their 1:1 physical mixture (SD1), and 1:1 SD formulation (SD6). The thermogram of the raw tacrolimus and its physical mixture with HPMC (SD1) showed a characteristic endotherm at 142 °C corresponds to the melting of tacrolimus. On the other hand, the SD formulation (SD6) exhibited no endothermic peak corresponding to tacrolimus, suggesting no crystallinity of tacrolimus in SD. From the results of XRD and DSC studies, it was confirmed that tacrolimus existed in an amorphous and crystalline states in its SD and physical mixture with HPMC, respectively. Mixing SD1 (100% crystalline drug) with SD6 (0% crystalline) at different proportions gave an array of partially crystalline SD formulations. The diffractograms of these formulations (SD1–SD6) showed a decrease in the intensity of the characteristic tacrolimus peaks corresponding to the level of the crystalline drug (Fig. 4A). The thermograms of SD1–SD6 showed a decreased in the intensity of the endothermic peak with a slight upward shift of the melting temperature by increasing the crystalline compartment within the SDs (Fig. 4B).

Assuming that the experimentally measured crystalline and amorphous X-ray intensities are proportional to the theoretical crystalline and amorphous fractions of the samples, the percentage crystallinity of SDs in the samples can be estimated using the following equation (Shah et al., 2006):

$$\%\,\text{Crystallinity} = \frac{100A_c}{A_c + A_a}$$

where A_c and A_a represent the respective area contributions from the crystalline and amorphous phases of the sample to the diffractograms, respectively. Although peak and halo intensities are sometimes used instead of areas, for this study, the comparison of the areas was used to minimize variations due to lattice strain and particle size. Using the collected data, the total area underneath the diffractograms (A_c and A_a) was calculated between 22.13° and 24.9° 2θ values using the trapezoidal rule, applied with Microsoft® Office Excel 2010 (Microsoft Corporation, Redmond, VA, USA). In order to

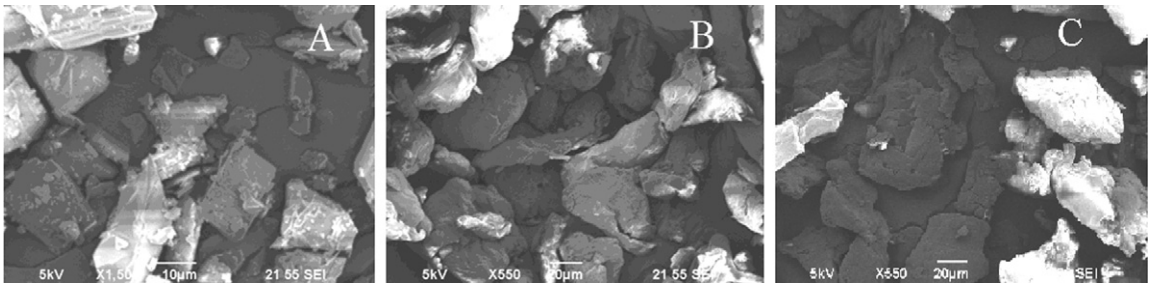

Fig. 2. Scanning electron micrographs: (A) tacrolimus powder (1500×), (B) HPMC powder (550×) and (C) their solid dispersion formulation, SD6 (550×).

separate contributions from the amorphous halo and the crystalline Bragg peaks (A_c), 5 points smoothing filtering was applied to the diffractograms using the Unscrambler software (version 9.5, CAMO ASA, Norway). The area underneath the Bragg peaks was then calculated separately from the overall area (De Gryze et al., 2007). The prediction of % crystallinity present in the samples were assessed by partial least squares (PLSs) models constructed using the same software. For the data collected, two PLS factors were found sufficient to regress the data without over-fitting. The results, shown as linear correlations between actual and predicted % crystallinity, are plotted in Fig. 5A. Using the same principle, the percentage crystallinity was determined from the thermograms of the SDs by calculating the percentage decrease in the heat of fusions (ΔH_f) by changing the theoretical crystalline fractions within the SD samples (Fig. 5B).

Fitting the DSC and XRD data to linear and third order polynomial fittings gave R^2 values of 0.9701, 0.9999 and 0.8974, 0.8740, respectively (Fig. 5). Despite the poor fit of both models, the actual versus the predicted plots from the PXRD data, 2θ range of 15–75°, gave better correlation compared to that from the DSC analysis. Fig. 5 shows a scatter from the linear correlation in the predicted % crystallinity from both PXRD and DSC data. This was especially apparent as the fraction of the crystalline drug in the sample was decreased, and the relative contribution from the Bragg peaks to the total area was decreased, and is reflected in the decreasing correlations (R^2) and increasing root mean squared errors of calibration and prediction (RMSEC and RMSEP) values (Table 1). For example, 5.3, 9.1 and 11.5, 27.1 were the RMSEs for calibration and prediction using either the XRD and DSC data, respectively. In addition, bias values of −0.33 and 7.9 were obtained for the prediction models of XRD and DSC data, respectively. Deviations of the calculated slopes from unity were also observed, indicating poor overall correlation between actual and predicted % crystallinity values using the current analysis specifications. Different variations of calculation methods based on the area underneath the diffractograms

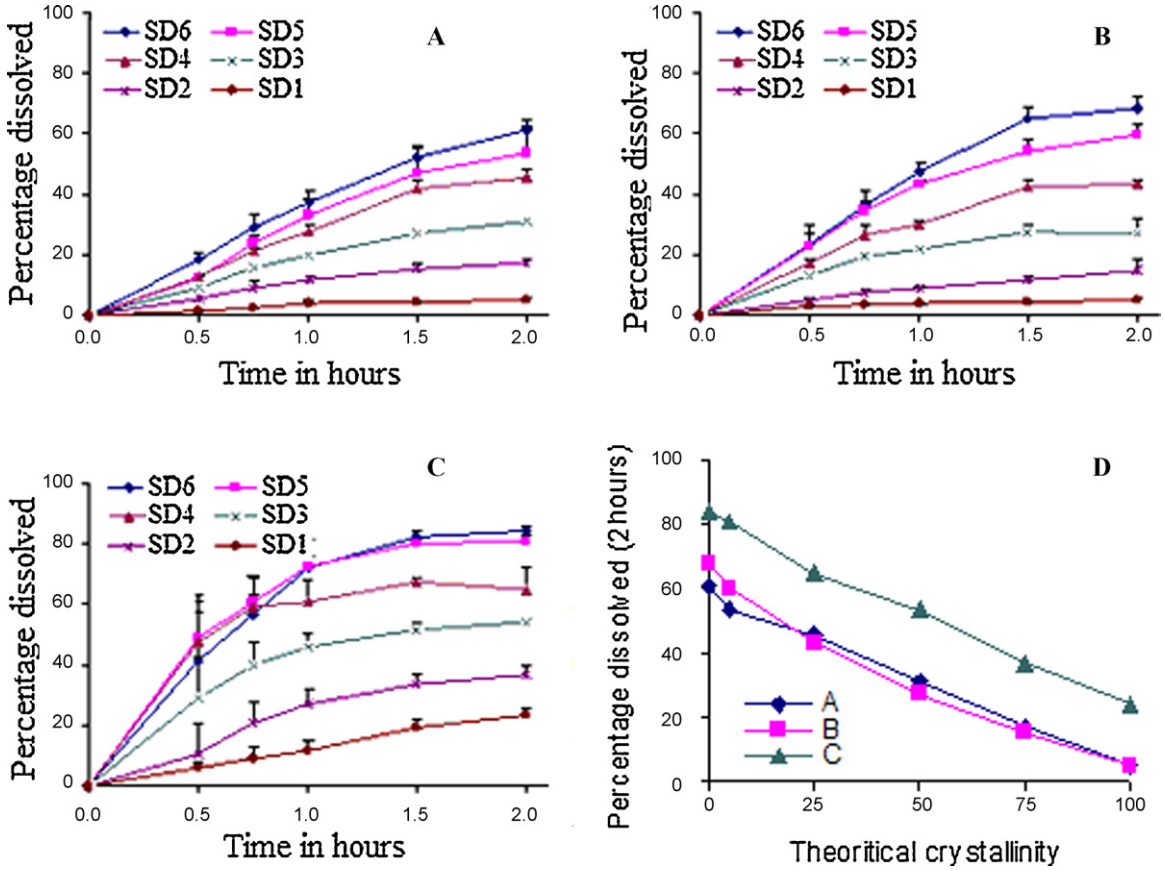

Fig. 3. Effect of dissolution condition on tacrolimus dissolution from SD formulations: (A) nominal dissolution conditions of 37 °C, 50 rpm with 900 ml of 0.005% HPC (pH 4.5), (B) dissolution at 75 rpm, (C) dissolution in 900 ml of 0.005% HPC (pH 4.5) having 0.01% SLS, and (D) the corresponding relationships between the percentage dissolved after 2 h and the theoretical crystallinity of the SDs.

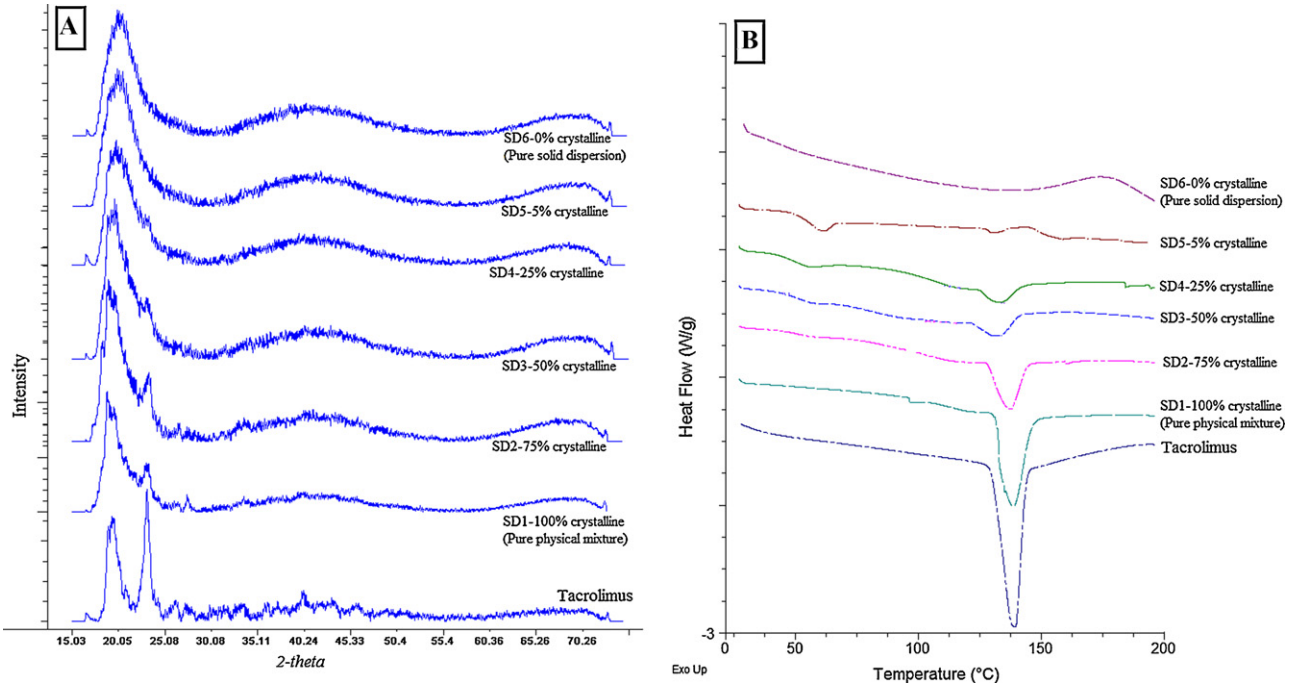

Fig. 4. Comparison of XRD patterns (A) and DSC thermograms (B) of raw tacrolimus, raw HPMC, 1:1 (w/w) physical mixture and different SD formulations of tacrolimus and HPMC at 6 crystallinity levels.

Table 1
Regression results from predicted versus actual values of the percentage crystallinity calculated from both the DSC and XRD data using the partial least square regression method.

	XRD data		DSC data	
	Calibration	Prediction	Calibration	Prediction
Slope	0.9782	0.9451	0.8985	1.1731
Offset	0.9239	1.9965	4.3134	0.5467
Correlation	0.9890	0.9682	0.9478	0.8619
R^2	0.9782	0.9564	0.8985	0.6157
RMSE[a]	5.3620	9.1096	11.587	27.056
SE[a]	5.8741	9.9724	12.693	28.347
Bias	-9.5×10^{-7}	−0.33	3.1×10^{-7}	7.92

[a] RMSE and SE are the root mean square errors and the standard errors of calibration or prediction, respectively.

were also attempted (data not shown). For example, correlations were attempted between % crystallinity of SDs and the total area underneath the diffractograms, as well as various different area normalization methods. None of the methods attempted improved the prediction abilities of the models. In addition, the linearity between actual and predicted % crystallinity was lost, such that the RMSEP values was unacceptably high (>25%) at either extreme of SD crystallinity percentages. In PXRD, the cause for the relatively large prediction errors might be poor signal-to-noise (S/N) ratio in the diffractograms with this 2-theta range. Increasing S/N ratio can be achieved by different ways such as increasing the scanning time and/or reducing the scan rate (Rumondor and Taylor, 2010); however none of them were successful with the current models. These results suggested that the used PXRD instrumentation has some limitations for the detection of the crystalline species within tacrolimus SDs. Better PXRD system with a higher sensitivity and wider 2θ range might give better correlations with improved precisions.

3.5. Raman spectroscopy

Raman bands are, in general, sharp, well-resolved and easily attributed to functional groups with some contributions due to the

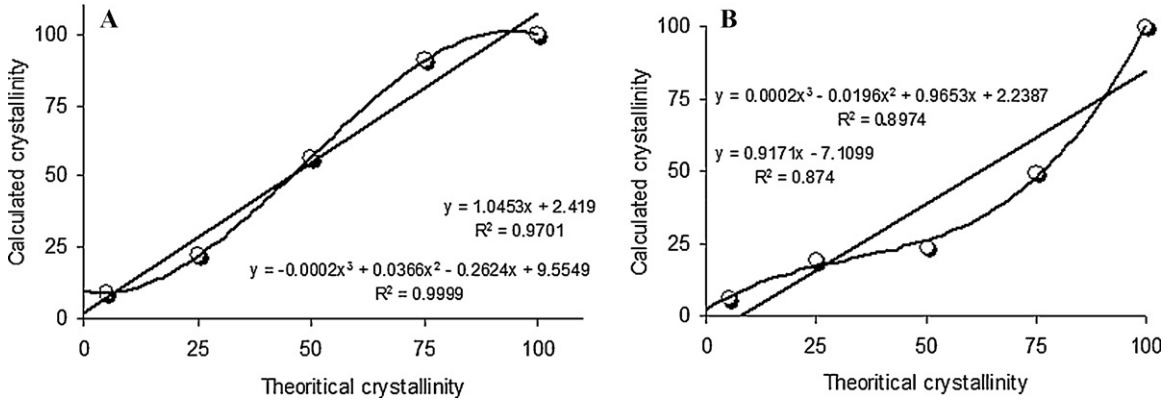

Fig. 5. Actual versus predicted % crystallinity in tacrolimus-HPMC SD samples containing 0, 5, 25, 50, 75, and 100% crystalline drug, as calculated from the proportional amorphous and crystalline contributions to the corresponding PXRD diffractograms (A) and DSC thermograms (B).

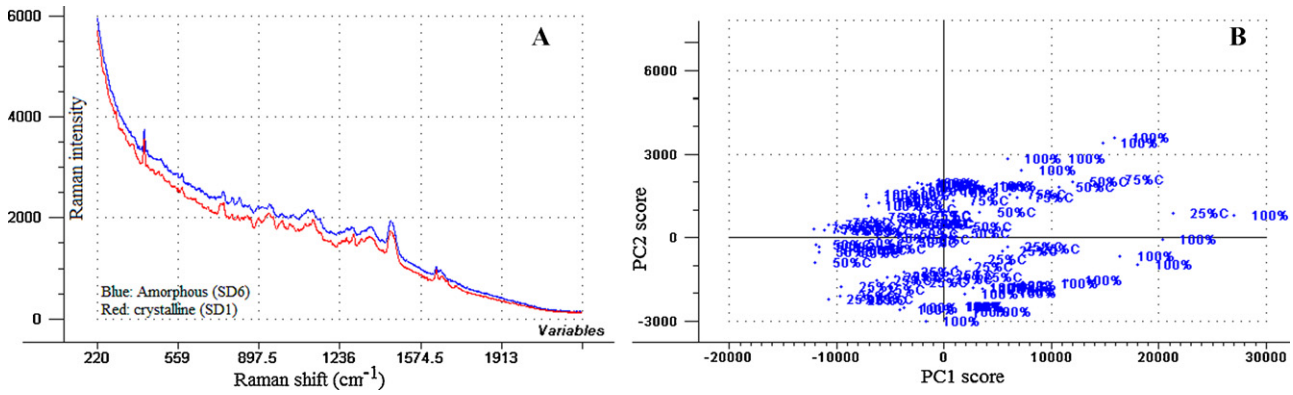

Fig. 6. Raman results: (A) Raman spectra of both the crystalline (SD1) and amorphous (SD6) fractions of SDs, and (B) Raman spectra of the SD formulations (20 replicates each) projected onto PC1 and PC2 scores computed by principle component analysis.

sample's crystallinity. A calibration model was developed for data obtained from off-line spectra of SD formulations. The performance of the calibration was evaluated based on the error values obtained from cross-validation. Fig. 6 shows the spectra for both the 100% crystalline (SD1) and 100% amorphous (SD6) fractions of the SDs. Characteristic peaks for the crystalline fraction were detected at 296.5, 316, 366.5, 735.5, 994, 1091 and 1661.5 cm^{-1}. Other SDs (SD2–SD5) spectra were in between these extremes with higher intensities for the peaks corresponding to the crystalline fractions as the crystallinity increased (spectra not shown). In an attempt to discriminate the six SDs based in their crystalline fractions, PCA was employed without any pretreatment of the spectra. Fig. 6B presents a score plot of 2 PCA factors, PC1 and PC2. Despite that these two factors were explaining 97% of the variability among the SDs (93% by PC1 and 4% by PC2), no specific clustering, trend or discrimination could be elucidated. Different score plots had been tried for the spectral data pretreated by normalization, derivatization or multiple scatter correction and none of them gave better result.

To construct a model for prediction, the changes in the shape and morphology of SD particles often cause variations and irregularities in baseline that were eliminated by applying a third order polynomial Savitzky–Golay second derivative conversion at 13 points smoothing. Table 2 summarizes the regression results to predict the percentage crystallinity within the SDs using a PLSR calibration model. The model was based on cross-validation using 60 Raman spectra (10 for each SD) for calibration and other 60 replicates for validation. Two PLS factors were employed for the prediction to explain about 94% of the constituted variability within the spectra. A linear fit could be obtained between the actual and predicted crystallinity with a slopes 0.95 and 0.59 and offsets of 2.1 and 20.7 for calibration and validation, respectively. Squared correlation coefficients of 0.9599 and 0.7902 were obtained with RMSE of 7.1% and 16.1% and SE of 7.1% and 16.3% for calibration and prediction, respectively. Compared to error percentages obtained from the DSC and PXRD calibration models, off-line Raman analysis might be able to predict the crystallinity of SDs better than DSC but not as good as PXRD. This can be attributed to the signal to noise ratio of Raman spectra which is not as good as that of PXRD diffractograms and the Raman spectra often include irregular noise (Shimoyama et al., 1997). In addition, it was not easy to select out a specific and precise wave number for a univariate chemometric analysis which reflects the changes in the crystallinity.

Table 2
Regression results from predicted versus actual values of the percentage crystallinity calculated from both Raman and NIR second derivative (third order polynomial) spectral data using the partial least square regression method.

	Raman data		NIR data	
	Calibration	Prediction	Calibration	Prediction
Slope	0.9599	0.5974	0.9932	1.0961
Offset	2.0	20.767	0.34	−13.9
Correlation	0.9797	0.9395	0.9965	0.9963
R^2	0.9599	0.7902	0.9932	0.9375
RMSE[a]	7.071	16.192	2.91	2.83
SE[a]	7.14	16.343	2.01	2.096
Bias	-1.14×10^{-7}	0.64	-5.08×10^{-7}	−4.11

[a] RMSE and SE are the root mean square errors and the standard errors of calibration or prediction, respectively.

3.6. NIR analysis

NIR spectroscopy is widely used in the chemical and pharmaceutical industry to assess the quality and the end-use properties of many products. It is therefore of major interest to evaluate to which extent NIR equipments could replace "usual analytical techniques" for quality control purposes. In this regard, NIR characterization of the sample crystallinity was compared with usual PXRD and DSC quantitative measurements. Fig. 7A shows the untreated NIR spectra of the SD formulations (6 spectra each). The most obvious NIR spectral change that occurred as a result of increasing the crystallinity of SDs was the upward shift in the spectral baseline. The baseline shift occurred across the spectrum, increasing in magnitude from the shorter wavelengths to the longer. In order to remove the baseline shifting and elucidate the peaks corresponding to both the crystalline and amorphous components of the SDs, third order polynomial Savitzky–Golay second derivative conversion at 13 points smoothing was employed. Comparison of the two second derivative spectra in Fig. 7A elucidated that the bands at 1406, 1508, 1784, 1906, 1962, and 2070 nm are attributed mainly to the crystalline fraction while the bands at 1340, 1704, 1914, 2064, and 2262 nm contributed from the amorphous component of SD. Fig. 7B shows the untreated spectra of the SDs projected onto PC1 and PC2 scores computed by principle component analysis. The 6 SDs were clustered using these two factors that explained 99% of the variability within these samples, 95% by PC1 and 4% by PC2, signified that the model for the characterization of SD crystallinity may be possible. Based on the PC1 score, the SDs were arranged according to increasing the crystallinity to speculate that PC1 and PC2 might refer to the crystalline and amorphous parts, respectively. Fig. 7C presents PC1 weight loadings plot that shows characteristic peaks at 1406, 1510, 1904, 1966, and 2070 nm to confirm that the score of PLS1 reflected the crystalline component of the SDs.

Results in Table 2 shows that regression via the PLS algorithm proved quite effective at providing a calibration model to predict percentage crystallinity within SD samples. When calibrating the model using 3 replicates out of 6 as training set samples, RMSEs

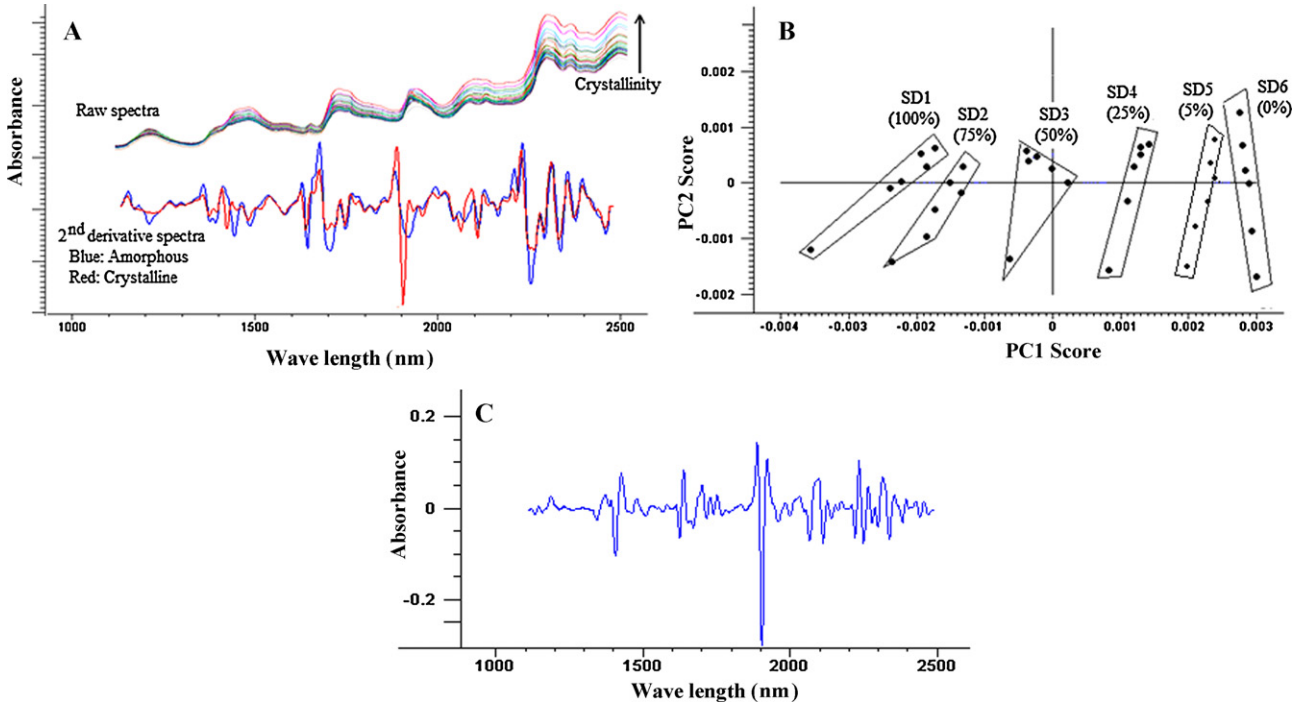

Fig. 7. NIR results: (A) NIR raw spectra of all the SDs and NIR second derivative spectra of the crystalline and amorphous fractions of SDs, (B) NIR spectra of the SD formulations (6 replicates each) projected onto PC1 and PC2 scores computed by principle component analysis, and (C) loading vector of PLS1.

of 2.91% and 2.83%, SEs of 2.01% and 2.09%, and squared correlation coefficients of 0.9965 and 0.9963 were obtained using 2 PLS factors for calibration and validation, respectively. Compared to PXRD, DSC and Raman models, accurate predictions for validation of the SD samples demonstrated that the NIR multivariate chemometric model has better capability of predicting the percentage crystallinity with percentage errors not exceeding 2%. Even though PXRD measurements provided the more accurate results than DSC and Raman analysis, it is clear that the quality of NIR spectroscopy measurements was satisfactory, with an average absolute uncertainty of the order of 2.1%, compared with PXRD. Considering the key advantages of NIR spectroscopy, it is clear that the technique is highly valuable as a product and process analytical tool.

3.7. NIR Imaging

The use of NIR imaging to perform mapping analysis on solid dispersion amorphous systems has been previously reported, especially to determine drug distribution in a matrix (Zidan et al., 2008; Rahman et al., 2010). NIR mapping data can be typically analyzed by: (i) integrating the characteristic band, (ii) ratioing the characteristic band intensities, or (iii) observing the full-width at half maximum of certain bands in order to distinguish crystalline and amorphous regions (Breitenbach et al., 1999; Docoslis et al., 2007; Furuyama et al., 2008). Although such spectral analysis can be useful to extract information on spatial distributions and to discriminate crystalline from amorphous phases, it may not give an accurate data analysis result especially when highly overlapping spectral bands are involved and when only subtle spectral differences exist between the amorphous and crystalline forms. In addition, such univariate analysis algorithms also tend to lose a lot of valuable full-spectrum information. In contrast, multivariate or chemometric analysis would allow for estimating the underlying pure component spectral estimates of observable components from the multicomponent mixture spectra data. In this prospect, a combined NIR imaging and multivariate or chemometric analysis was used in the current study to characterize the crystallinity of SD formulations. Spectral data analysis presented is similar to the one carried out on the data extracted from a typical NIR spectroscopy. The percentages of crystalline fraction obtained for the 6 SDs in each pixel of the scanned samples using PLSR are shown in Fig. 8A. Visual observation of the images indicated that neither the presence of aggregates nor agglomeration of the individual components of the system, tacrolimus and HPMC, was observed, which revealed a correct distribution of the drug at the surface of the SD measured, enhancing the correct dissemination and thus heading towards a homogeneous distribution. The mean signal concentration values for crystalline drug were close to the theoretical concentration in the SD. The variation between different images of the same sample (measured with the standard deviation and the coefficient of variation) was within acceptable limits, allowing the correct matching between the theoretical concentration and the concentration obtained with PLSR model.

Similar pixel concentration distributions of the crystalline drug were observed for all the SDs. This fact is enhanced by the similar values of skewness and kurtosis (results not shown) obtained for all the samples. In fact, there were two clear distributions. Some pixels had low concentration of the crystalline drug which might indicate that it was in a low concentration at the measured surface. On the other hand, the pixels with higher amount of the crystalline drug formed a Gaussian distribution with a mean value corresponding to the crystallinity of the sample. Comparing the enriched spectral character of crystalline drug in the high intensity pixels in the six SDs, one could arrange them in the correct ranking based on the theoretical percentage crystallinity. A quantile–quantile plot was constructed for the actual percentage crystallinity and the percentage contribution of the crystalline fraction within the pixels using the PLSR score images (Fig. 8B). A good correlation with coefficients of 0.9888 for first order and 0.9896 for second order polynomial relationships was obtained explaining the validity

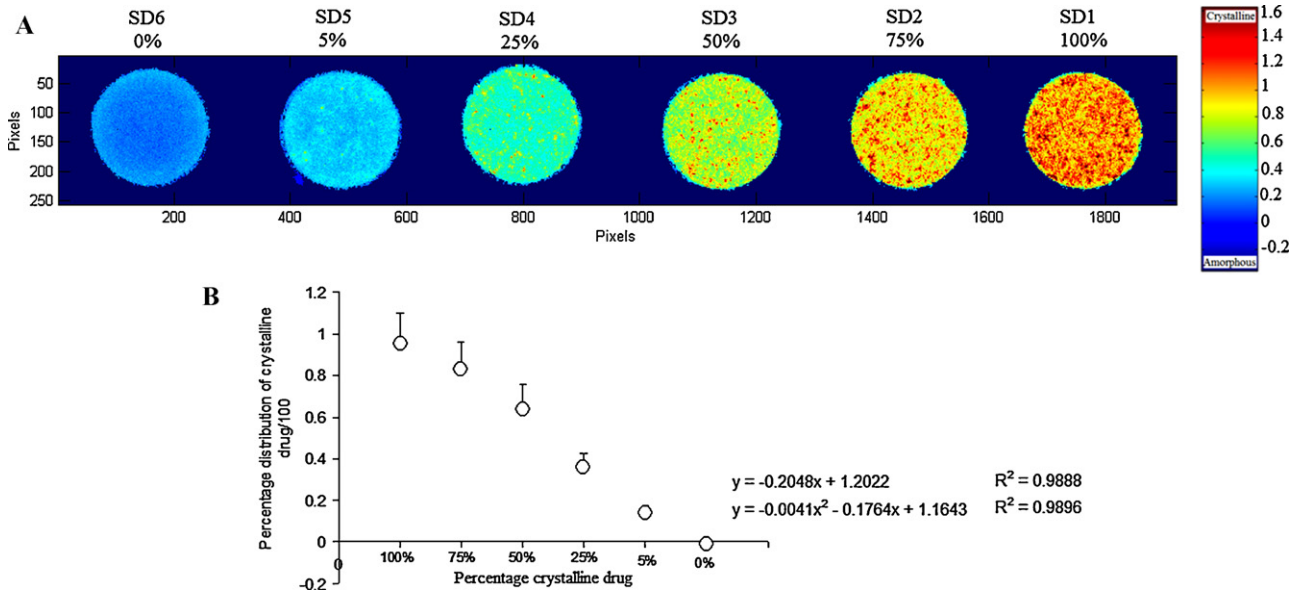

Fig. 8. NIR imaging results: (A) concatenated PLSR concentration images for the SD formulations, the color scale indicates the percentage of the crystalline fraction in each pixel of the scanned surface, and (B) the quantile–quantile plot for predicting the percentage crystallinity using the PLS score images' pixels intensities truncated at 50×100 pixels each.

of the PLSR imaging model for the nondestructive crystallinity assessment within tacrolimus SD formulations.

4. Conclusion

The tacrolimus SDs with HPMC prepared by the solvent evaporation technique were used as a model for monitoring the drug crystallization behavior. The performance of PXRD, DSC, Raman, NIR or NIR imaging coupled with chemometric analysis were evaluated as methods to detect the crystallinity of the drug within SDs. Results obtained show that drug crystallinity in amorphous molecular-level SDs could be well estimated quantitatively and spatially through the application of PLSR to the NIR spectra, while the other methods yielded calibration models with less sensitivity. Moreover, this nondestructive method required less subjective and time intensive data analysis, since it can be performed on the data without the need to separate the contributions from the included excipients or the amorphous fractions.

Acknowledgments

The authors would like to thank the Oak Ridge Institute for Science and Education (ORISE) for supporting the post doctoral research program.

References

Adams, M.J., 1995. Chemometrics in Analytical Spectroscopy, RSC, Analytical Spectroscopy Monographs. The Royal Society of Chemistry, Cambridge, UK, p. 216.
Awa, K., Okumura, T., Shinzawa, H., Otsuka, M., Ozaki, Y., 2008. Self-modeling curve resolution (SMCR) analysis of near-infrared (NIR) imaging data of pharmaceutical tablets. Anal. Chim. Acta 619, 81–86.
Berendt, R.T., Sperger, D.M., Isbester, P.K., Munson, E.J., 2006. Solid-state NMR spectroscopy in pharmaceutical research and analysis. Trends Anal. Chem. 25, 977–984.
Breitenbach, J., Schrof, W., Neumann, J., 1999. Confocal Raman-spectroscopy: analytical approach to solid dispersions and mapping of drugs. Pharm. Res. 16, 1109–1113.
Breitenbach, J., 2002. Melt extrusion: from process to drug delivery technology. Eur. J. Pharm. Biopharm. 54, 107–117.
Chiou, W.L., Riegelman, S., 1971. Pharmaceutical applications of solid dispersion systems. J. Pharm. Sci. 60, 1281–1302.
Cho, S., Chung, H., Lee, Y., 2005. Simple and fast near-infrared spectroscopic analysis of hydroxyl number of polyol using a disposable glass vial. Microchem. J. 80, 189–193.
Crowley, K.J., Zografi, G., 2003. The effect of low concentrations of molecularly dispersed poly(vinylpyrrolidone) on indomethacin crystallization from the amorphous state. Pharm. Res. 20, 1417–1422.
De Gryze, S., Langhans, I., Vandebroek, M., 2007. Using the correct intervals for prediction: a tutorial on tolerance intervals for ordinary least-squares regression. Chemom. Intell. Lab. Syst. 87, 147–154.
Docoslis, A., Huszarik, K.L., Papageorgiou, G.Z., Bikiaris, D., Stergiou, A., Georgarakis, E., 2007. Characterization of the distribution, polymorphism, and stability of nimodipine in its solid dispersions in polyethylene glycol by micro-Raman spectroscopy and powder X-ray diffraction. AAPS J. 9, E361–E370.
Elkhider, N., Chan, K.L.A., Kazarian, S.G., 2007. Effect of moisture and pressure on tablet compaction studied with FTIR spectroscopic imaging. J. Pharm. Sci. 96, 351–360.
Furuyama, N., Hasegawa, S., Hamaura, T., Yada, S., Nakagami, H., Yonemochi, E., 2008. Evaluation of solid dispersions on a molecular level by the Raman mapping technique. Int. J. Pharm. 361, 12–18.
Hancock, B.C., Zografi, G., 1997. Characteristics and significance of the amorphous state in pharmaceutical systems. J. Pharm. Sci. 86, 1–12.
Hane, K., Fujioka, M., Namiki, Y., Kitagawa, T., Kihara, N., Shimatani, K., Yasuda, T., 1992. Physico-chemical properties of (−)-1R,9S,12S,13R,14S,17R,18E,21S,23S,24R,25S,27R)-17-allyl-1,14-dihydroxy-12-[(E)-2-[(1R,3R,4R)-4-hydroxy-3-methoxycyclohexyl]-1-methylvinyl]-23,25-dimethoxy-13,19,21,27-tetrametyl-11,28-dioxa-4-azatricyclo[22.3.1.04,9]octacos-18-ene-2,3,10,16-tetrone hydrate (FK-506). Iyakuhin Kenkyu 23, 33–43.
Honbo, T., Kobayashi, M., Hane, K., Hata, T., Ueda, Y., 1987. The oral dosage form of FK-506. Transpl. Proc. 19, 17–22.
Hooks, M.A., 1994. Tacrolimus, a new immunosuppressant – a review of the literature. Ann. Pharmacother. 28, 501–511.
Kushida, I., Ichikawa, M., Asakawa, N., 2002. Improvement of dissolution and oral absorption of ER-34122, a poorly water-soluble dual 5-lipoxygenase/cyclooxygenase inhibitor with anti-inflammatory activity by preparing solid dispersion. J. Pharm. Sci. 91, 258–266.
Law, D., Krill, S.L., Schmitt, E.A., Fort, J.J., Qiu, Y., Wang, W., Porter, W.R., 2001. Physicochemical considerations in the preparation of amorphous ritonavir-poly(ethylene glycol) 8000 solid dispersions. J. Pharm. Sci. 90, 1015–1025.
Leuner, C., Dressman, J., 2000. Improving drug solubility for oral delivery using solid dispersions. Eur. J. Pharm. Biopharm. 50, 47–60.
Lin, W.Q., Jiang, J.H., Yang, H.F., Ozaki, Y., Shen, G.L., Yu, R.Q., 2006. Characterization of chloramphenicol palmitate drug polymorphs by Raman mapping with multivariate image segmentation using a spatial directed agglomeration clustering method. Anal. Chem. 78, 6003–6011.
Loser, K., Balkow, S., Higuchi, T., Apelt, J., Kuhn, A., Luger, T.A., Beissert, S., 2006. FK506 controls CD40L-induced systemic autoimmunity in mice. J. Invest. Dermatol. 126, 1307–1315.
Miyazaki, T., Yoshioka, S., Aso, Y., Kawanishi, T., 2007. Crystallization rate of amorphous nifedipine analogues unrelated to the glass transition temperature. Int. J. Pharm. 336, 191–195.

Naes, T., Isaksson, T., Fearn, T., Davies, T., 2002. A User-friendly Guide to Multivariate Calibration and Classification. NIR Publications, Chichester, UK, p. 420.
Rahman, Z., Zidan, A.S., Khan, M.A., 2010. Risperidone solid dispersion for orally disintegrating tablet: its formulation design and non-destructive methods of evaluation. Int. J Pharm. 400, 49–58.
Roggo, Y., Chalus, P., Maurer, L., Lema-Martinez, C., Edmond, A., Jent, N., 2007. A review of near infrared spectroscopy and chemometrics in pharmaceutical technologies. J. Pharm. Biomed. Anal. 44, 683–700.
Rumondor, A.C.F., Taylor, L.S., 2010. Application of partial least-squares (PLS) modeling in quantifying drug crystallinity in amorphous solid dispersions. Int. J. Pharm. 398, 155–160.
Shah, B., Kakumanu, V.K., Bansal, A.K., 2006. Analytical techniques for quantification of amorphous/crystalline phase in pharmaceutical solids. J. Pharm. Sci. 95, 1641–1665.
Shimoyama, M., Maeda, H., Matsukawa, K., Inoue, H., Ninomiya, T., Ozaki, Y., 1997. Discrimination of ethylene/vinyl acetate copolymers with different composition and prediction of the vinyl acetate content in the copolymers using Fourier-transform Raman spectroscopy and multivariate data analysis. Vib. Spectrosc. 14, 253–259.
Sugimoto, I., Sasaki, K., Kuchiki, A., Ishihara, T., Nakagawa, H., 1982. Stability and bioavailability of nifedipine in fine granules. Chem. Pharm. Bull. 30, 4479–4488.
Tamura, S., Tokunaga, Y., Ibuki, R., Amidon, G.L., Sezaki, H., Yamashita, S., 2003. The site-specific transport and metabolism of tacrolimus in rat small intestine. J. Pharmacol. Exp. Ther. 306, 310–316.
Tishmack, P.A., Bugay, D.E., Byrn, S.R., 2003. Solid-state nuclear magnetic resonance spectroscopy-pharmaceutical applications. J. Pharm. Sci. 92, 441–474.
Venkataramanan, R., Shaw, L.M., Sarkozi, L., Mullins, R., Pirsch, J., MacFarlane, G., Scheller, D., Ersfeld, D., Frick, M., Fitzsimmons, W.E., Virji, M., Jain, A., Brayman, K.L., Shaked, A., 2001. Clinical utility of monitoring tacrolimus blood concentrations in liver transplant patients. J. Clin. Pharmacol. 41, 542–551.
Venkataramanan, R., Swaminathan, A., Prasad, T., Jain, A., Zuckerman, S., Warty, V., McMichael, J., Lever, J., Burckart, G., Starzl, T., 1995. Clinical pharmacokinetics of tacrolimus. Clin. Pharmacokinet. 29, 404–430.
Vippagunta, S.R., Maul, K.A., Tallavajhala, S., Grant, D.J.W., 2002. Solid-state characterization of nifedipine solid dispersions. Int. J. Pharm. 236, 111–123.
Waldrep, J.C., 1998. New aerosol drug delivery systems for the treatment of immune-mediated pulmonary diseases. Drugs Today 34, 549–561.
Watanabe, T., Wakiyama, N., Usui, F., Ikeda, M., Isobe, T., Senna, M., 2001. Stability of amorphous indomethacin compounded with silica. Int. J. Pharm. 226, 81–91.
Willart, J.F., Descamps, M., 2008. Solid state amorphization of pharmaceuticals. Mol. Pharm. 5, 905–920.
Yamashita, K., Nakate, T., Okimoto, K., Ohike, A., Tokunaga, Y., Ibuki, R., Higaki, K., Kimura, T., 2003. Establishment of new preparation method for solid dispersion formulation of tacrolimus. Int. J. Pharm. 267, 79–91.
Yonemochi, E., Kitahara, S., Maeda, S., Yamamura, S., Oguchi, T., Yamamoto, K., 1999. Physicochemical properties of amorphous clarithromycin obtained by grinding and spray drying. Eur. J. Pharm. Sci. 7, 331–338.
Yoshihashi, Y., Iijima, H., Yonemochi, E., Terada, K., 2006. Estimation of physical stability of amorphous solid dispersion using differential scanning calorimetry. J. Therm. Anal. Calorim. 85, 689–692.
Yoshioka, S., Aso, Y., 2007. Correlations between molecular mobility and chemical stability during storage of amorphous pharmaceuticals. J. Pharm. Sci. 96, 960–981.
Zidan, A.S., Habib, M.J., Khan, M.A., 2008. Process analytical technology: nondestructive evaluation of cyclosporine A and phospholipid solid dispersions by near infrared spectroscopy and imaging. J. Pharm. Sci. 97, 3388–3399.